

# Manufacturing and ultimate mechanical performance of carbon fibre-reinforced epoxy composite suspension push-rods for a Formula 1 racing car

M. D. GILCHRIST and L. CURLEY

*Mechanical Engineering Department, University College Dublin, Belfield, Dublin 4, Ireland*

**ABSTRACT** The contemporary Formula 1 racing car makes extensive use of advanced composite materials in its construction. The design, manufacture and ultimate performance under compression of composite suspension push-rods, that typically could be used in a Grand Prix racing car, are described in this present paper. An aerofoil cross-section has been used based on different lay-ups of carbon/epoxy composite. One push-rod was manufactured using a uniform layup of unidirectional and woven cross-ply prepreg, whilst a further three push-rods were manufactured with a tapered layup of unidirectional and woven cross-ply prepreg. Failure mechanisms including fibre microbuckling, fibre kinking and fibre fracture were observed, whilst comparisons have been made between the experimentally observed failure strains and those that were predicted using simple buckling theory. The ultimate compressive strength of the structural component was significantly less than that of the carbon/epoxy composite.

**Keywords** Suspension push-rod; Formula 1 racing car; Compression loading; Carbon/epoxy composite; Fracture; Buckling.

## **NOMENCLATURE**

$a$  = half-major axis of ellipse  
 $A$  = cross-sectional area of push-rod  
 $b$  = half-minor axis of ellipse  
 $E$  = stiffness (Young's modulus)  
 $G$  = stiffness (shear modulus)  
 $I$  = moment of inertia  
 $K$  = buckling coefficient (=0.7 for one end pinned and one end fixed, and 1.0 for both ends pinned)  
 $L$  = length of push-rod (=650 mm)  
 $P$  = actuator load  
 $r$  = smallest radius of gyration  
 $\nu$  = Poisson's ratio  
 $\sigma$  = stress

### *Subscripts*

cr = critical  
ext = external  
int = internal  
11 = longitudinal  
22 = transverse

## **INTRODUCTION**

More than 80% of a modern Formula 1 car is made from some form of composite material, with the majority

of components being based on carbon/epoxy systems. Such extensive use of advanced materials originates back to the mid-1970s, when the 'wing-car', developed by Lotus, created large downward forces by using the

underside of the car. This required large wing-shaped underbodies to be attached to a chassis of reduced width, the torsional rigidity of which could only be maintained efficiently by using composite materials. Additionally, turbochargers emerged in the late 1970s, and producing thrusts in excess of 1400 BHP, these led to severe loads being applied to the chassis. Composite materials offered greater specific stiffnesses and greater flexibility in design than the aluminium alloys that had been used previously.

A central load-bearing structure in a modern F1 car connects the front and rear suspension systems; this load-bearing structure consists of the monocoque, engine and gearbox casing. The driver, fuel tank and front suspension dampers are housed within the monocoque, whilst the engine is jointed to the back of the monocoque on four studs. The gearbox casing is attached to the rear face of the engine. This three-piece box-beam structure carries the inertial loads to the four corners of the car. Various wing structures, underbodies, cooler ducting and bodywork are attached to and around this box-beam.

The first carbon fibre-reinforced epoxy polymer monocoque was moulded in 1981 for the McLaren MP4 F1 car. The monocoque was moulded over a machined aluminium tool which was subsequently removed in sections through the cockpit opening. Unidirectional carbon/epoxy was used for the skins, whilst aluminium honeycomb was used for the core. This design was used in a form that remained virtually unchanged for six racing seasons, so successful was the one-piece construction. A two-piece construction was pioneered by Gustav Brunner in 1983 for his ATS F1 car by moulding the monocoque as top and bottom halves in a female mould. This provided advantages of greater flexibility with respect to the geometry and size of the monocoque over the one-piece construction.

More recently, however, composites have begun to be used to manufacture components other than primary structural parts, e.g. high-strength components, the gearbox casing, where torsional rigidity is crucial, and suspension components, which require high stiffness. Traditional metal suspension components are being replaced by composites in order to increase the stiffness of the individual suspension members, and thereby give the designer more control over the overall stiffness of the suspension system. It is the push-rod which has the single major influence on the stiffness of the suspension system. However, the change from metal to composite components has not been without problems for many F1 teams. Williams, e.g. replaced the metal push-rod by a composite push-rod, but had to revert to the metal component due to a series of rear suspension failures in testing.

This particular paper aims to investigate the performance of a composite push-rod under compression and,

through representative experimental tests, to assist design engineers in predicting the ultimate limits to which a composite push-rod could be used. The geometry and stacking sequence that were used to manufacture the push-rods of the present work are discussed, as is the experimental test set-up that was used to apply direct compression to the components. The performance of the push-rods under compression, the manner of failure and the fracture mechanisms that were observed are also discussed.

## DESIGN AND MANUFACTURE OF COMPONENTS

### Push-rod design

In order to minimize the effects of wind-drag around the push-rods, it was decided to utilize an aerofoil cross-section instead of a circular cross-section. Uniform and tapered layups were used, the purpose of the taper being to increase the equivalent modulus along the critical section of the push-rod and consequently, to increase the load at which buckling would occur. Since the end sections of both the tapered and uniform layups were identical, it was anticipated that the load at which compression failure should occur would be identical for both types of push-rod. The push-rod was 650 mm long, whilst the nominal wall thickness was 1.825 mm for the uniform push-rod, and varied between 1.825 and 2.450 mm for the tapered push-rods. The major and minor external dimensions of the airfoil axes were nominally specified at  $38 \times 18$  mm.

One objective of this project was to investigate the influence of the layup on the possible buckling response of the push-rod. Since the principal in-service mechanical load on the push-rod was uniaxial compression, it was necessary to maximize the number of  $0^\circ$  plies within the stacking sequence in order to provide maximum uniaxial stiffness. A number of cross-plyies were necessary, however, to prevent longitudinal splitting of the push-rod. The first stacking sequence that was considered was a uniform layup of  $(0^\circ/90^\circ; 0^\circ; 0^\circ/90^\circ)$ , i.e. two external  $0^\circ/90^\circ$  cross-plyies of woven prepreg surrounding nine unidirectional  $0^\circ$  plies. This layup differs from that which is typically used in current F1 design only in that there are no tapered plies within the stacking sequence. As such, it was anticipated that the ultimate mechanical response of this push-rod design would be a lower bound limit and failure would be due to buckling.

The remaining three push-rods were identically tapered along their midlengths and the particular stacking sequence that was used was  $(0^\circ/90^\circ; 0^\circ; 90^\circ; 0^\circ; 0^\circ/90^\circ)$ , i.e. two outer  $0^\circ/90^\circ$  cross-plyies of woven prepreg surrounding seven  $0^\circ$  plies, one  $90^\circ$  ply and six  $0^\circ$  plies. The taper was obtained by only placing some of the  $0^\circ$

**Table 1** Mechanical properties of the 0°/90° woven and unidirectional carbon/epoxy material systems used to manufacture the composite push-rods

Mechanical property	0°/90° woven ply	Unidirectional ply
Thickness	0.35 mm	0.125 mm
Longitudinal stiffness	53 GPa	310 GPa
Transverse stiffness	52 GPa	5.9 GPa
Shear modulus	0.011 GPa	0.012 GPa
Poisson's ratio, $\nu_{12}$	0.1	0.2
Longitudinal tensile strength	690 MPa	1960 MPa
Longitudinal compressive strength	59 MPa	700 MPa
Transverse tensile strength	690 MPa	354 MPa
Transverse compressive strength	59 MPa	354 MPa
Shear strength	80 MPa	100 MPa

**Table 2** Equivalent mechanical properties of uniform and tapered layups used to manufacture the different push-rods

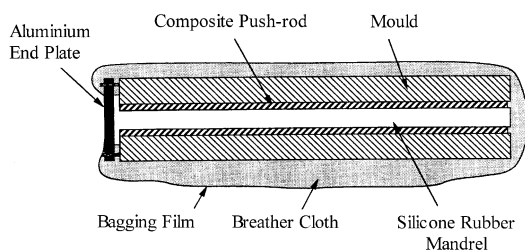
Equivalent laminate property	Uniform layup	Tapered layup
Longitudinal stiffness, $E_{11}$	211 GPa	221 GPa
Transverse stiffness, $E_{22}$	23.7 GPa	34.7 GPa
Poisson's ratio, $\nu_{12}$	0.115	0.068
Poisson's ratio, $\nu_{21}$	0.013	0.011
Shear modulus, $G_{12}$	11.6 MPa	11.7 MPa

and 90° plies along part of the 650 mm length of the push-rods.

Commercially available laminate analysis software was used [1] to estimate equivalent laminate properties and strengths from the precise ply properties of Table 1. The values of these equivalent laminate properties are detailed in Table 2.

### Push-rod manufacture

Three separate carbon/epoxy push-rods were manufactured by wrapping the various plies of prepreg around a hollow elliptical silicone mandrel. This was then placed within an elliptical two-part cavity mould and cured in an autoclave, as shown in Fig. 1. The hollow mandrel

**Fig. 1** The autoclave moulding arrangement used to manufacture the push-rods.

acted as an expandable bladder during the curing cycle, thereby pressing the prepreg firmly against the walls of the mould and ensuring that a uniform wall thickness was produced along the length of the push-rod.

The autoclave curing cycle for the woven and unidirectional carbon/epoxy prepreg involved a 1.5 h cure at 125 °C and 700 kPa with a heat-up and cool-down rate of 3 °C/min. When the temperature reached 125 °C, the vacuum was vented to atmosphere. Pressure was then introduced and ramped at 100 kPa/min to 700 kPa. When the pressure cycle was completed, the pressure was ramped down at 50 kPa/min to 0 kPa, at which stage the vacuum was reintroduced.

Both the mould and silicone mandrel were reused when manufacturing all three push-rods, and these were cleaned and degreased before being coated with release agent (FreeKote) prior to the plies of carbon/epoxy prepreg being wrapped around the mandrel and placed within the mould. Figure 1 illustrates how the complete assembly was vacuum bagged to evacuate air, solvents and entrapped volatiles from the laminate, and to allow the positive autoclave pressure to consolidate the laminate against the mould surface. A breather cloth bagging assembly was used to absorb any excess resin flow and also to smooth out the sharp corners of the mould, which could cause the vacuum bag to rupture under the high autoclave pressures. A solid release film was placed against the mould walls to prevent the breather cloth from sticking to the mould surfaces. Upon completion of the curing cycle, the vacuum bag assembly was removed from the autoclave. The bag and breather were discarded and the end plates were removed prior to the mould being opened. The composite push-rod was then taken from the mould and the silicone mandrel removed from the centre of the push-rod.

Before the actual carbon/epoxy push-rods could be manufactured, it was necessary to manufacture a suitable elliptical mould and elliptical silicone mandrel so that the finished push-rods would be of the required thickness and cross-section. The mould was machined from aluminium, whilst the silicone mandrel was manufactured using GFRP slips, an elliptical copper pipe and the mould, as shown schematically in Fig. 2. The copper pipe was located centrally within the mould cavity through an aluminium end-plate. The end-plate was subsequently bolted to the mould and the mould was inverted. The GFRP slips were placed against the mould walls, and de-aerated liquid silicone rubber was poured into the space between the GFRP slips and the copper pipe in the mould. This assembly was left under room conditions for 14 h to allow the rubber compound to cure, and was then placed in an oven at 120 °C for 1.5 h to complete the curing process. The hollow silicone mandrel was then removed from the mould and the

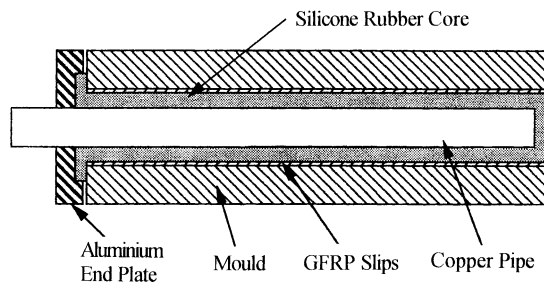


Fig. 2 Arrangement of the mould assembly for manufacturing the hollow silicone mandrel.

copper pipe was extracted from the mandrel. No significant air bubbles or voids, which would have made the mandrel unsuitable for manufacturing the push-rods, were detected visually.

The GFRP slips were fabricated using the two halves of the mould. After spraying release agent on both halves of the mould, six plies of GFRP were stacked in each half of the mould. The two halves of the mould were covered in a release ply, covered with a bleeder cloth and placed in a vacuum bag, which was then sealed. The assembly was placed in the autoclave and cured using an appropriate curing cycle.

A fourth carbon/epoxy push-rod was manufactured using a sandbag technique instead of the silicone mandrel, which ruptured when being removed from the third push-rod. The procedure involved in making this core used a cylindrical nylon tube (thermally stable, thin and impermeable). The mould, with the GFRP slips, was then bolted together and the nylon tube was inserted into the mould cavity. The tube was sealed at one end using sealant tape, and dry sand was then added to the tube and compacted by means of a vacuum pump. The subsequent procedure for manufacturing this fourth push-rod was identical to that based on using the silicone mandrel.

However, this fourth push-rod was laid up incorrectly with a slight overlap in the first ply, which prevented the first ply from expanding and consolidating against the other plies in the mould during the autoclaving process. This prevented resin from flowing to the surface and consequently exposed fibres were detected at the outer surface of the push-rod after manufacture. In normal operating conditions such a component would be scrapped. Nevertheless, this push-rod was tested in the same manner as the other three push-rods, and the results of all four tests are discussed in the following sections.

## EXPERIMENTAL TEST SET-UP

Four push-rods have been tested statically to failure under compression using a displacement mode of control

on a 100 kN uniaxial servohydraulic fatigue machine (Series 8501 Instron). The loading was introduced at both ends of a push-rod using female end-fixtures which had been designed to provide boundary conditions that were pin-jointed at the bottom and cantilevered at the top in order to simulate in-service support conditions. This is shown schematically in Fig. 3.

Surface strains, from gauges at three different positions on the push-rods, were recorded using a data acquisition system which operated on a keypress sequence. Strain gauges were aligned longitudinally and transversely along the length of the push-rods to measure the performance under compressive load. Two gauges [SG1 and SG2 of Fig. 4(a)–(d)] were aligned axially at the midlength and on opposite faces of the push-rods: these provided information on the presence of buckling, the deviation from linearity in the mechanical response of the push-rod, and the fracture strains. A third strain gauge [not included in Fig. 4(a)–(d)] was aligned normal to the first two gauges, close to the midlength position of the push-rod, and was used to calculate values of Poisson's ratio.

## RESPONSE OF PUSH-RODS UNDER STATIC COMPRESSIVE LOADS

### Introduction

All push-rods were loaded statically to failure by means of a displacement mode of control. Load, displacement and strain values were collated at discrete increments of actuator load. As the applied load was increased from

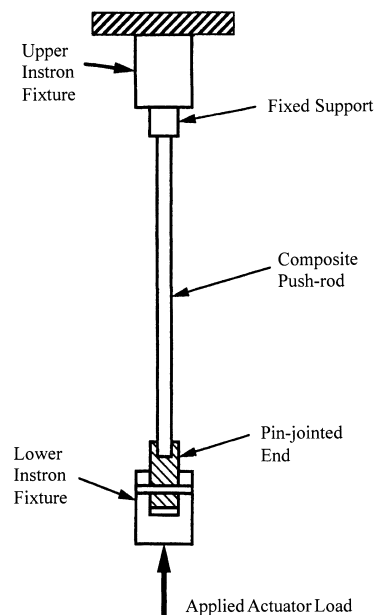
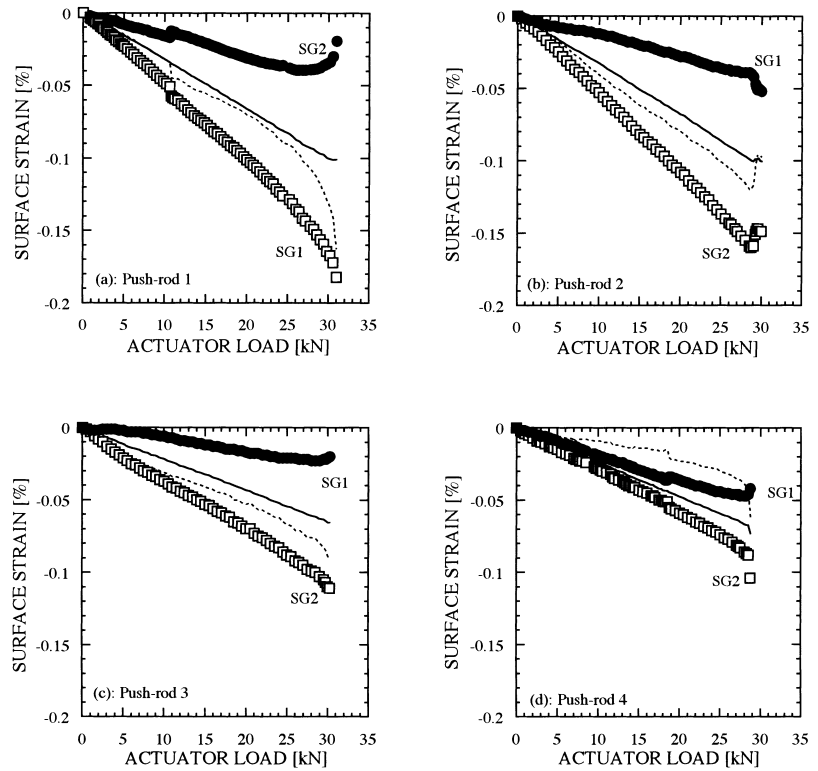


Fig. 3 Compression test set-up used to establish the ultimate performance of the carbon/epoxy push-rods.



**Fig. 4** Variation of surface strains with actuator load during testing of push-rods 1–4 [(a)–(d), respectively]. Buckling is identified by the difference between the values of the two surface strain readings, and starts with the onset of actuator load. Incipient fracture is identified by the deviation of strain differences from linearity, which occurs at  $\approx 90\%$  of the ultimate failure load in all four tests. The solid and dashed lines represent average strains and strain differences, respectively.

zero, the response of the push-rods was initially linear elastic. Figure 4(a)–(d) details the variation of compressive surface strains at the midlength position on opposite sides of the four push-rods with increasing actuator load. The strain responses deviated from linearity at  $\approx 90\%$  of the final failure load, although minor fracture events occurred before this deviation from linearity in the first and fourth push-rod tests [minor fracture events occurred at 10.8 kN in Fig. 4(a) and 18.75 kN in Fig. 4(d), respectively]. This deviation of strain difference (i.e. magnitude of strain difference between front and back faces of the push-rods =  $SG2 - SG1$ ) from linearity, which occurred at  $\approx 90\%$  of the final failure load, identified the onset of catastrophic fracture. Ultimate failure of the first uniformly laid-up push-rod occurred some 40 mm from the centre of the specimen, whilst failure of the remaining three push-rods was concentrated around the bottom ends of the specimens, close to the pin-jointed end-fixtures of the testing machine. Table 3 details the loads and strains at which ultimate failure and deviation from linearity occurred during the four push-rod tests.

The measured actuator loads and surface strains are presented in Fig. 4(a)–(d) for the four push-rods. The average load–strain relationship for all the push-rods is essentially linear almost until fracture. However, the individual strain gauge readings deviate from linearity immediately with the application of load, and this devi-

ation continues to increase directly with applied load up until failure.

Table 3 identifies the maximum direct compressive strains which were measured during each test and may be compared against the failure strains of the carbon fibres of 1.5% [2]. While the maximum direct strain reading at the failure of push-rod 1 (i.e. 0.18%) is greater than those recorded during the other three tests (this is to be expected as the strain gauge position of this push-rod was closer to the failure site than in all other tests), this is considerably less than the fibre failure strain. Consequently, failure of these components is considered to be due to geometric and manufacturing factors rather than material limitations.

### Buckling behaviour

A simple first mode of buckling was apparent along the length of the four test specimens, with maximum lateral deformation (i.e. crest of the buckle) occurring close to the midlength of the push-rods. Buckling initiated with the application of load in all the push-rod tests, as can be seen from the deviation of the two sets of surface strain gauge readings [Fig. 4(a)–(d)] from the average compressive strain. The amplitude of the buckle increased linearly in magnitude with actuator load until failure. No dial gauges were used during the tests to quantify the amplitude of the buckle, although this could

Specimen/ Push-rod number	Actuator load at deviation from linearity (kN)	Ultimate failure conditions		
		Actuator load (kN)	Surface strain (%)	Location
PR1	25.40	31.00	0.182	40 mm from midlength
PR2	28.50	30.00	0.160	pin-joint end
PR3	28.50	30.25	0.111	pin-joint end
PR4	26.50	28.75	0.104	pin-joint end

**Table 3** Summary of experimental test data [cf. Figure 4(a)–(d)]

be estimated from the degree of bending that has been measured by the surface strain gauges.

### Damage in beams

The compressive failure mechanisms that occurred in all four push-rods were similar, although failure of push-rod 1 occurred at a position close to the midlength of the component, whereas failure was close to the pin-jointed end for the other three push-rods. The reason for this different failure site is due to the fact that push-rod 1 was manufactured without any tapered region in its midsection, unlike the other three push-rods. The general appearance of the fracture associated with push-rod 4, which is similar to that observed in the other push-rods, is shown in Fig. 5. The appearance of the fracture surface is different both around the perimeter of the push-rod and through the thickness of the push-rod. The fracture is not uniformly compressive around the perimeter, this is due to the different degrees of compressive strains that existed on opposite sides of the push-rod. The lack of similarity of the through-thickness fracture features is partly due to the variation of compressive strains and partly due to the different ply orientations through the thickness of the push-rod. Figures 6–8 detail the compressive failure sites that led to ultimate fracture of the push-rods, as identified using scanning electron microscopy. Many buckled and broken

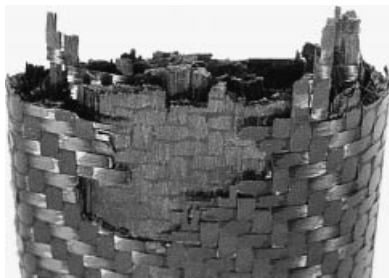


**Fig. 5** Compressive fracture of push-rod 4 as identified visually. The outer 0°/90° woven ply is clearly visible. The damage mechanism that initiated failure was due to compressive stress (far side in the photograph). The external diameter and thickness of this push-rod are 38 mm and 18 mm, respectively.

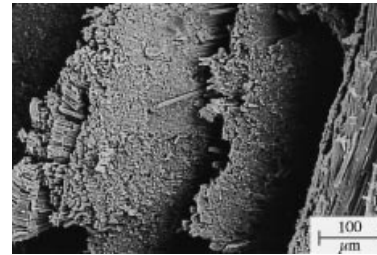


**Fig. 6** Global view micrograph of compressive fracture of the push-rod identifying crushed fibre ends and fibre kinking, fibre microbuckling and fibre fracture.

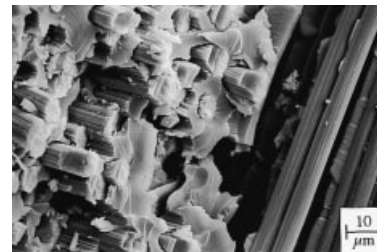


**Fig. 7** Local view micrograph of compressively fractured fibres.

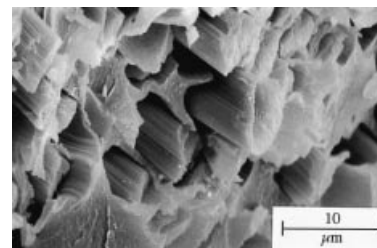


**Fig. 8** Local view micrograph of fracture surfaces of fibre ends. Note the degree of poor fibre-matrix adhesion where the fibres are debonded from the epoxy resin.

fibres and crushed fibre ends are evident in Fig. 6, and the manner in which these fibres fractured is characteristic of compressive failure, i.e. fibre microbuckling and localized fibre fracture [3–9].

## PREDICTIONS OF PUSH-ROD BEHAVIOUR

Using simple Euler buckling theory it was possible to predict the loads and strains associated with buckling by approximating the airfoil cross-section with that of an ellipse:

$$\sigma_{cr} = \frac{\pi E}{(KL/r)^2}$$

where  $r$ , the smallest radius of gyration, is defined by

$$r = \sqrt{I/A}$$

For push-rod 1 (PR1), classical laminate theory predicts a longitudinal modulus of 211 GPa (cf. Table 2). The moment of inertia is calculated from the half-major and half-minor dimensions of the cross-section of the push-rod. These external dimensions are 18.87 mm and 8.94 mm, whilst the corresponding internal dimensions are 17.05 mm and 7.12 mm, respectively. Consequently, the moment of inertia of PR1 is given as:

$$I_{PR1} = \frac{\pi}{4} (a_{ext} b_{ext}^3 - a_{int} b_{int}^3) = 5756 \text{ mm}^4$$

Similarly, the cross-sectional area of PR1 is calculated as 148.6 mm<sup>2</sup>. In order to calculate both the critical buckling load and the surface strains within the push-rod at this corresponding level of load, it is necessary to determine the correct buckling coefficient,  $K$ , for the particular boundary conditions that are applied to the push-rod ends. The nominal boundary conditions, selected to represent what would typically occur in service, define one end as pinned and allowed to rotate about this point, and the other end as fixed and prevented from any displacements or rotations about this point. For such a case, the buckling coefficient  $K=0.7$ . However, the physical conditions within the constrained end of the push-rod are not quite as severe and are actually insufficient to prevent rotation: this is because of the fact that the push-rod is hollow with a relatively thin wall section and the interior walls of the push-rod are not prevented from rotating in towards the middle of the push-rod. This particular arrangement did not permit the fixed boundary condition to transfer bending moments into the push-rod. Consequently, it is more realistic to consider that the actual boundary conditions were closer to both ends being pinned ( $K=1$ ) than to one end being fixed and the other being pinned ( $K=0.7$ ). On this basis, the critical buckling load,  $P_{cr} = 57.9$  kN if  $K=0.7$ , and  $P_{cr} = 28.4$  kN if  $K=1$ . The corresponding levels of surface strain would be 0.19% if  $K=0.7$  and 0.09% if  $K=1$ . These values compare quite

well with the average strain of 0.10% and the failure load of 31.0 kN for push-rod 1.

The half-major and half-minor external and internal dimensions of tapered push-rods PR2–PR4 were 18.87, 8.94, 16.42 and 6.49 mm, respectively. The moment of inertia and cross-sectional area were therefore calculated as 7064 mm<sup>4</sup> and 195.2 mm<sup>2</sup>, respectively. The critical buckling load  $P_{cr} = 74.4$  kN if  $K=0.7$ , and  $P_{cr} = 36.5$  kN if  $K=1$ . The corresponding levels of surface strain are 0.17% and 0.08%. These values compare relatively well with the failure loads identified in Table 3 and the average strains of Fig. 4(b)–(d).

## DISCUSSION

A conventionally designed tubular steel cylindrical push-rod, which could be of 26 mm external diameter and 2 mm wall thickness, would have a critical buckling load of  $P_{cr} = 30.1$  kN and average surface strain of 0.18% for  $K=1$ . The corresponding weight of such a push-rod would be 0.383 kg (density = 7500 kg/m<sup>3</sup>). This is compared against the composite push-rods of the present paper which would be of similar strength and stiffness but would also be some 50% lighter and would weigh  $\approx 0.203$  kg (density  $\approx 1600$  kg/m<sup>3</sup>).

While it is clear that composite suspension push-rods can be designed and manufactured to provide equal stiffness and strength characteristics to conventional steel push-rods, and at the same time offer some degree of weight saving, it is necessary to realize that other issues are important in deciding whether current metallic materials could be replaced safely by high-performance composites. The amount of energy absorption by the suspension system in the event of an accident to the corner of a car, e.g. may well establish that plastic deformation occurring in wishbone tubes outperforms a more brittle mode of fracture in a composite system. In other cases, the reasons for using a composite system might not be structural but could be due to aerodynamic factors where the flexibility of manufacturing from composites permits greater geometric freedom.

## CONCLUSIONS

Unidirectional and woven cross-ply carbon/epoxy composites were used to manufacture suspension push-rods that could typically be used in a Formula 1 racing car. These were subsequently loaded to failure under compression using end boundary conditions which approximated those that would be used typically in service. Three push-rods had a tapered midsection consisting of 0° and 90° plies, whilst an initial trial specimen was of constant thickness along its length. The results of this investigation can be summarized as follows:

- (1) Fracture of the trial specimen (push-rod 1) occurred close to the midlength, whilst fracture in all other cases was close to the pin-jointed support in the loading frame. Buckling occurred in all cases and this increased directly with the application of load.
- (2) The ultimate performance of these particular push-rods was limited by geometric, manufacturing and support parameters, and fracture occurred at load levels that were far less than the ultimate fibre failure strains of the materials that were used. Consequently, it is possible that, with redesign, additional improvements in performance could be obtained.
- (3) While these composite push-rods offer valuable weight savings over conventional steel push-rods for Formula 1 motor racing without compromising strength and stiffness, it is important that issues, e.g. manufacturing complexity and crashworthiness, are evaluated thoroughly before conventional engineering materials are replaced by high-performance composite materials.

### Acknowledgements

The authors would like to acknowledge Mr J. McQuillan of Jordan Grand Prix for providing materials, Mr J. Mallon of University College Dublin for carrying out aspects of the experimental work, and Mr B. O'Rourke of Williams Grand Prix Engineering for useful discussions. Financial support provided by means of a

President's Research Award from University College Dublin is gratefully acknowledged.

### REFERENCES

- 1 LAP (1991) Laminate Analysis Program, Centre for Composite Materials, Imperial College, London SW7 2BY, UK.
- 2 D. R. Lovell (1991) *Carbon and High Performance Fibres Directory*, 5th edn. Chapman & Hall.
- 3 M. D. Gilchrist and N. Svensson (1995) A fractographic analysis of delamination within multidirectional carbon/epoxy laminates. *Comp. Sci. Technol.* **55**, 195–207.
- 4 M. D. Gilchrist, A. J. Kinloch, F. L. Matthews and S. O. Osiyemi (1996) Mechanical performance of carbon fibre and glass fibre-reinforced epoxy I-beams: I—Mechanical behaviour. *Comp. Sci. Technol.* **56**, 37–53.
- 5 M. D. Gilchrist, A. J. Kinloch and F. L. Matthews (1996) Mechanical performance of carbon-fibre and glass-fibre reinforced epoxy I-beams: II—Fractographic failure observations. *Comp. Sci. Technol.* **56**, 1031–1045.
- 6 N. Svensson, R. Shishoo and M. D. Gilchrist (1998) Fabrication and mechanical response of commingled GF/PET composites. *Polymer Comp.* **19**, 360–369.
- 7 M. D. Gilchrist, N. Svensson and R. Shishoo (1998) Fracture and fatigue performance of textile commingled yarn composites. *J. Mater. Sci.* **33**, 4049–4058.
- 8 M. D. Gilchrist, N. Svensson and R. Shishoo (1998) Interlaminar fracture of commingled GF/PET laminates. *J. Comp. Mater.* **32**, 1808–1835.
- 9 N. Svensson and M. D. Gilchrist (1998) Mixed mode delamination of multidirectional carbon fibre/epoxy laminates. *Mech. Comp. Mater. Struct.* **5**, 291–307.